Structural, electrical, and optical properties of $CuGaSe_2$ rf sputtered thin films

I. Mártil, J. Santamaria, G. Gonzalez Diaz, and F. Sanchez Quesada
Departamento Electricidad y Electronica. Fac. Ciencias Fisicas, Universidad Complutense, 28040 Madrid, Spain

(Received 4 December 1989; accepted for publication 22 February 1990)

Thin films of $CuGaSe_2$ have been produced by rf sputtering. Compositional, structural, electrical, and optical properties are strongly influenced by growth temperature. At substrate temperatures lower than 300 °C amorphous or poorly crystalline Se-excess films are obtained, showing high resistivity ($\approx 10^3\ \Omega$ cm) and optical transitions at 1.62, 1.80, and 2.4 eV (values lower than the single-crystal counterparts). At the higher growth temperatures, polycrystalline films are obtained (average grain size 0.7 μm) with lower values of resistivity (1 Ω cm), and optical transitions at 1.68, 1.90, and 2.55 eV (very close to the single-crystal values). A hopping conduction mechanism has been detected at the lower measuring temperature ($T < 150$ K), and a grain boundary limited conduction process at the higher measurements temperature ($T > 150$ K). Structural and compositional characteristics are used to explain the behavior observed in the electrical and optical properties.

I. INTRODUCTION

The $CuGaSe_2$ (CGS) chalcopyrite semiconductor is near the ideal partner for the $CuInSe_2$ semiconductor in tandem structures.[1] While the physical properties of $CuInSe_2$ thin films grown by several techniques are now well established, CGS thin films have been less studied.

There are reports on electrical and optical properties of CGS films grown by compound evaporation,[2] elemental constituent evaporation,[3] flash evaporation,[4] selenization,[5] etc., showing electrical properties of CGS thin films to be strongly influenced by film composition[3] and by the presence of crystallographic phases other than tetragonal CGS.[6] Optical characterization has revealed[4,7] a complex band structure, with several transitions between valence-band subbands and the conduction band. According to our knowledge, such studies have not been conducted on CGS sputtered films. Sputtering is a low-cost thin-film deposition technique, which in dealing with other similar materials, such as $CuInSe_2$, has yielded thin films with properties similar to those of films produced by other techniques. We have recently reported the first results on physical properties of CGS film produced by rf sputtering.[8] In this paper we present results on structural, electrical, and optical properties of rf sputtered CGS thin films.

II. EXPERIMENT

CGS films were obtained by sputtering from a compound target with 2% Se excess (at. %) in a rf diode sputtering system (G.C.A. Vacuum Industries) previously described.[9] The CGS target was obtained by reacting elemental, high-purity components in a vacuum-sealed quartz ampoule. The compound was reduced to fine powder (particle size $< 40\ \mu$m), cold pressed, and bonded to an oxygen-free high-conductivity copper (OFHC) block. Further details about the target preparation can be found in Ref. 8.

Sputtering gas pressure and target voltage were kept constant at 20 mTorr (and 900 V, respectively); substrate temperature ranged between 60 and 400 °C; the substrate holder was electrically floating and the target-to-substrate distance was set at 5 cm. Substrates were glass slides ultrasonically cleaned in a tricloroethane-acetone-methanol cycle, rinsed in de-ionized water, and dryed in a N_2 flux. Film thicknesses ranged between 0.5 and 3 μm, as measured by a Sloan–Dektak profile analyzer. The growth rate showed a monotonic decrease when substrate temperature was increased. At 60 °C, the growth rate was 140 Å/min and at 400 °C it was 85 Å/min.

Film characterization consisted of X-ray diffraction (XRD) measurements (Siemens Difractometer) to identify crystallographic phases and degree of structural disorder, scanning electron microscopy (SEM) observations, and energy dispersive X-ray analysis (EDAX) composition analysis (JEOL-JSM 35-C, scanning electron microscope); resistivity measurements were made with variable temperature in the range of 100–450 K (The Van Der Pauw method was used on 1-cm side square geometries). Samples had four Au evaporated electrodes in the corners. Also, thermoelectric measurements (hot-probe method) were performed to obtain information about conductivity type. Finally, transmittance measurements were done in the spectral range 2.5–0.4 μm (Perkin–Elmer Lambda 9 spectrophotometer). Refractive index and absorption coefficient were obtained from transmittance data using the method described in Ref. 10. The refractive index in the low-absorption zone was deduced from the positions of maxima and minima in the transmittance spectra. Transmittance values and refractive index extrapolated after the Sellmeier dispersion rule were used to obtain the absorption coefficient in the high-absorption region of the spectrum.

III. RESULTS AND DISCUSSION

A. Structure and composition

Depending on the growth temperature, three different types of films could be distinguished:

(a) Films grown at temperatures lower than 200 °C do not exhibit any reflection in XRD patterns or a broad reflec-

 0021-8979/90/130189-06$03.00

tion at $2\theta = 27.7°$ corresponding to the (112) plane of the CGS tetragonal structure. In Fig. 1(a) we present an XRD pattern of a representative film grown at 170 °C. The broad peak observed seems to indicate the amorphous structure of these films. SEM observations did not reveal any surface structure, in accordance with this conclusion.

(b) Films grown at temperatures between 200 and 300 °C showed the presence of several CGS tetragonal structure reflections and additional reflections characteristic of the δ-GaSe binary phase structure. An XRD pattern of a film grown at 244 °C is presented in Fig. 1(b) clearly showing the presence of the binary phase.[11] The high Se and Ga content of these films (see below, Fig. 2) seems to promote the δ-GaSe binary phase formation. Similar results have been reported for Ga excess evaporated CGS films.[12]

(c) Films grown at temperatures higher than 300 °C showed sharp, well-defined, reflections characteristic of the CGS tetragonal structure with no presence of binary phases. In Fig. 1(c), the XRD pattern of a film grown at 330 °C is shown. Single-phase CGS is observed, with a strong (112) preferential orientation. SEM observations of this third group of CGS films revealed average grain sizes in the range 0.5–0.9 μm, for temperatures ranging between 330 and 400 °C.

EDAX analysis showed the composition to be strongly influenced by the growth temperature, as shown in Fig. 2, for the Se/Cu + Ga ratio; the Cu/Ga ratio, on the other hand, remained practically unaffected when the substrate temperature was changed, the films being always Ga rich.

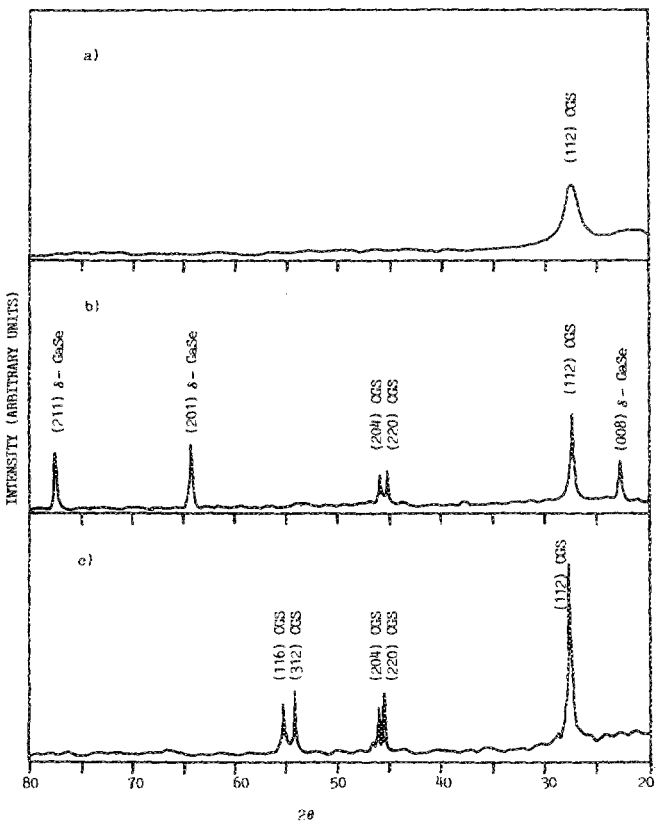

FIG. 1. XRD patterns of three representative films grown at (a) 170 °C, (b) 244 °C, and (c) 330 °C. The diagrams show the different phases present in the films. Thicknesses are similar for the three samples (~ 1 μm).

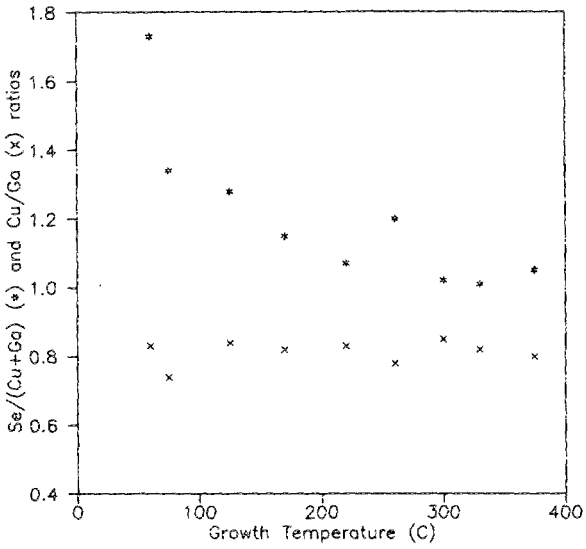

FIG. 2. Se/Cu + Ga and Cu/Ga ratios vs growth temperature.

B. Electrical properties

All the films analyzed exhibited p-type conductivity, as shown by hot-probe experiments, with no measurable Hall effect. Film resistivity was strongly influenced by the growth temperature, showing a pronounced decrease when the substrate temperature was raised. Results are presented in Fig. 3. Changes of resistivity can be due either to changes in composition and consequently in the carrier density, or to structural effects (structural disorder can be responsible for a reduced mobility). In order to highlight this point and to get information about the conduction mechanism of films, measurements of resistivity at variable temperatures have been performed, for films grown at various growth temperatures. It is well known that polycrystalline semiconductors exhibit a temperature dependence of resistivity that, according with several proposed models, can be expressed as[13,14]

$$\rho = \left(\sqrt{2\pi m_p^* kT}/q^2 lp\right) \exp(\Delta E/KT), \qquad (1)$$

where m_p^* is the effective mass, l is the average grain size, T is

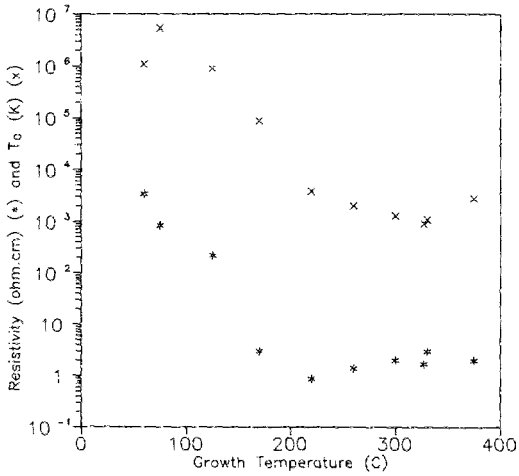

FIG. 3. Values of the resistivity and T_0 parameter in Eq. (2) as a function of the growth temperature.

the absolute temperature, k is Boltzmann's constant, q is the electron charge, p is the average free-carrier concentration, and $\Delta E = (E_v - F) + \Phi_b$. In this last expression Φ_b is the height of the intercrystalline barrier at grain boundaries measured from the top of the valence band, E_v is the top of the valence-band energy, and F is the Fermi level.

According to this equation, we have plotted in Fig. 4 $\rho/\sqrt{T}$ data vs $1000/T$ for two representative films grown at substrate temperatures of 75 and 320 °C, respectively. For measurement temperatures higher than 150 K, data can be fitted to straight lines, indicating, in accordance with Eq. (1), thermal emission over the intercrystalline barrier and thermal generation of carriers from acceptors levels. The presence of various slopes in the $\rho/\sqrt{T}$ vs $1000/T$ characteristics, points to thermal activation of carriers from different levels to the valence band; in fact, acceptor levels located at 30, 50, 110, 150, 180, and 380 meV above the top of the valence band have been described in the literature.[4,15,16] Since acceptor levels and their population are closely related to stoichiometry defects (see Fig. 2), both structure (intercrystalline barrier) and composition can be invoked to explain the electrical characteristics of our films. Unfortunately a nonmeasurable Hall effect makes a separation of both effects not possible.

At the lower measurement temperature, on the other hand, the electrical conduction process is not thermally activated. An analysis of resistivity data in this temperature range revealed the presence of a hopping conduction mechanism[17] for which the resistivity shows the temperature dependence quoted in Eq. 2,

$$\rho = \sqrt{\gamma T / A^2 N(E_F)}\, \exp[(T_0/T)^{1/4}] \qquad (2)$$

where $N(E_F)$ is the density of localized states around the Fermi level, γ is a measure of the spacial extension of the wave function associated with those states, and A is a constant. Plots of $\rho/\sqrt{T}$ vs $(1/T^{1/4})$ in semilogarithmic scale, for the two films of the preceeding paragraph (see Fig. 5), yielded straight lines, thus supporting the presence of such a mechanism in our films for the measurement temperatures lower than 150 K.

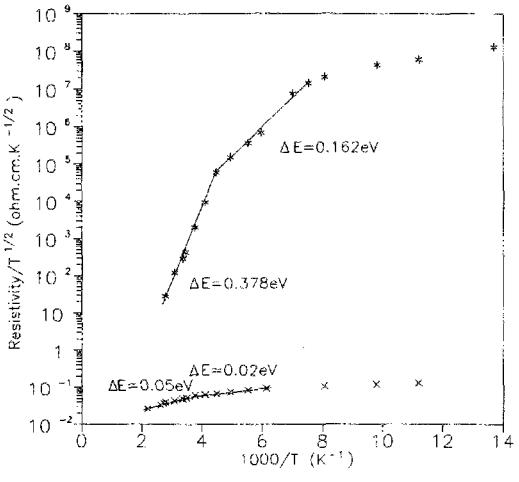

FIG. 4. Variation of resistivity with the measurement temperature ($\log \rho/\sqrt{T}$ vs $1000/T$) for films grown at 75 °C (*) and 320 °C (×).

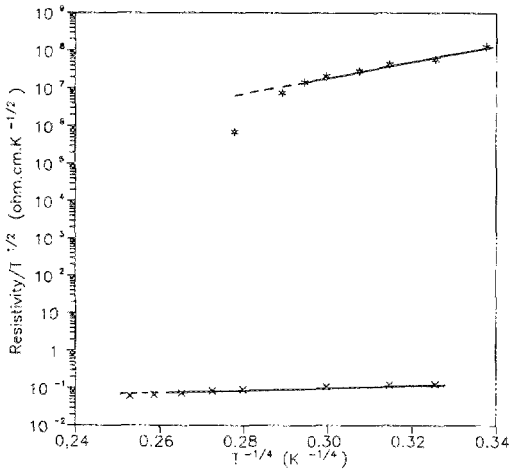

FIG. 5. Variation of resistivity with the temperature, at the lower measurement temperature [$\log \rho/\sqrt{T}$ vs $(1/T)^{1/4}$] for films of Fig. 4, grown at: 75 °C (*) and 320 °C (×).

The T_0 factor in Eq. (2) is directly related to the structural disorder of the films,[18] i.e., the density of gap states through which the conduction process takes place. T_0 values obtained for all the films analyzed are plotted versus the growth temperature in Fig. 3.

The high T_0 values, ranging between 10^5 and 10^6 K, obtained at the lower growth temperature, are well in the range reported for amorphous semiconductors,[18] and allow an explanation of the high-resistivity values obtained at the lower growth temperature in terms of the disordered structure of CGS films, already established in the structure section (Sec. III A) after XRD measurements and SEM observations.

At the higher growth temperature, on the other hand, T_0 values in the range 10^3 K, characteristic of polycrystalline semiconductors,[19] were obtained. The decrease observed in T_0 also correlates very well with the decrease in the resistivity values, as shown for both parameters in Fig. 3. The decrease observed in the Se/Cu + Ga ratio, on the other hand, also fits reasonably well with the decay of the resistivity.

We conclude therefore that both compositional and structural characteristics are mainly responsible for the behavior observed in the resistivity values when the growth temperature was changed.

C. Optical properties

In Fig. 6, we show data of refractive index of a representative film grown at 327 °C as a function of the photon energy. Single-crystal values, after Ref. 20, are also presented. The slightly lower values obtained for the sputtered films are probably due to the lower density of thin films than the single-crystal counterpart.[21] No clear correlation between refractive index and production conditions was found.

Absorption coefficient of a film grown at 330 °C is shown in Fig. 7. For clarity, only few experimental points have been plotted in the figure. A detailed analysis of the absorption coefficient data revealed the presence of several optical transitions, as observed by several authors.[2,4,7] In

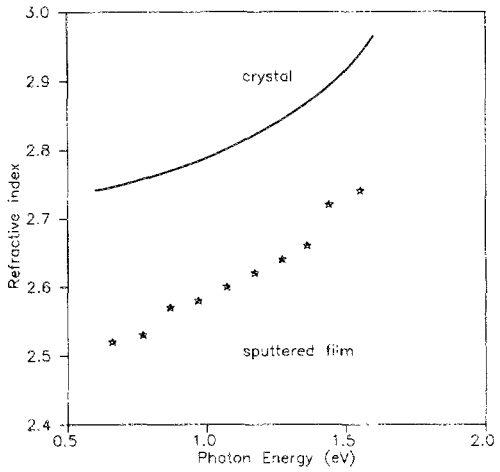

FIG. 6. Refractive index vs photon energy for a representative film grown at 327 °C and for a single crystal (Ref. 20).

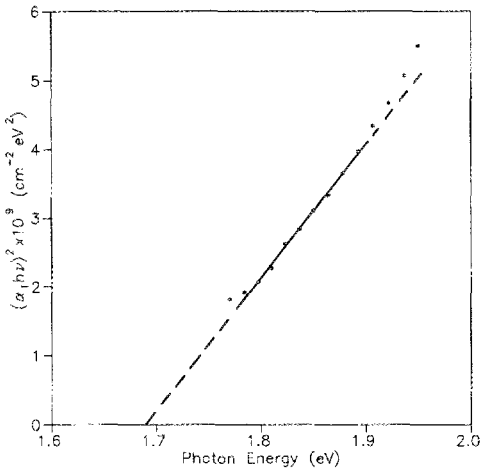

FIG. 8. Replot of data in Fig. 7 [$(\alpha_1 h\nu)^2$ vs $h\nu$]. The extrapolation of linear part indicates the presence of the allowed direct fundamental transition at 1.69 eV [Eq. (3)].

fact, for energies lower than 1.90 eV, the absorption coefficient can be expressed in the form

$$\alpha_1 = (A_1/h\nu)\ (h\nu - E_g)^{1/2}, \tag{3}$$

indicating the presence of the fundamental allowed direct transition. The data are presented in Fig. 8. An energy gap value of $E_f = 1.69$ eV is deduced by extrapolation of the $(\alpha_1 h\nu)^2$ vs $h\nu$ characteristic to $(\alpha_1 h\nu)^2 = 0$. This gap value is in very good agreement with the commonly accepted gap value of 1.68 eV for CGS single crystals.[22]

Additional absorption processes for higher energies can be seen in Fig. 8. For energies in the range 1.90 eV $< h\nu <$ 2.30 eV, additional absorption can be attributed to the presence of forbidden direct transitions. In this energy range, absorption coefficient can be expressed as follows:

$$\alpha_2 = \alpha_{\text{exp}} - \alpha_1 = (A_2/h\nu)\ (h\nu - E_f)^{3/2}, \tag{4}$$

where α_{exp} is the absorption coefficient experimentally obtained from transmittance measurements and E_f is the energy for that this forbidden direct transition takes place.

Results are presented in Fig. 9(a) An E_f value of 1.90 eV was deduced, very close to the value of 1.92 eV reported

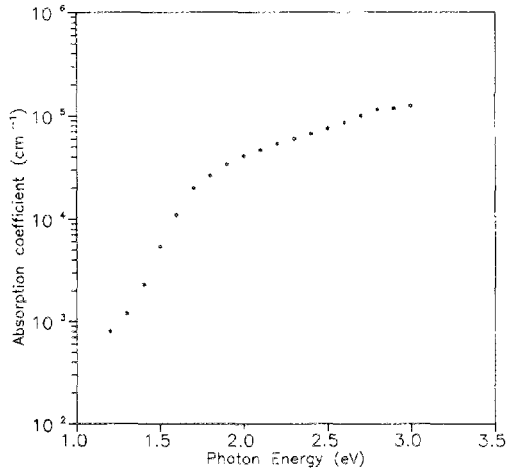

FIG. 7. Absorption coefficient vs photon energy for a film grown at 330 °C.

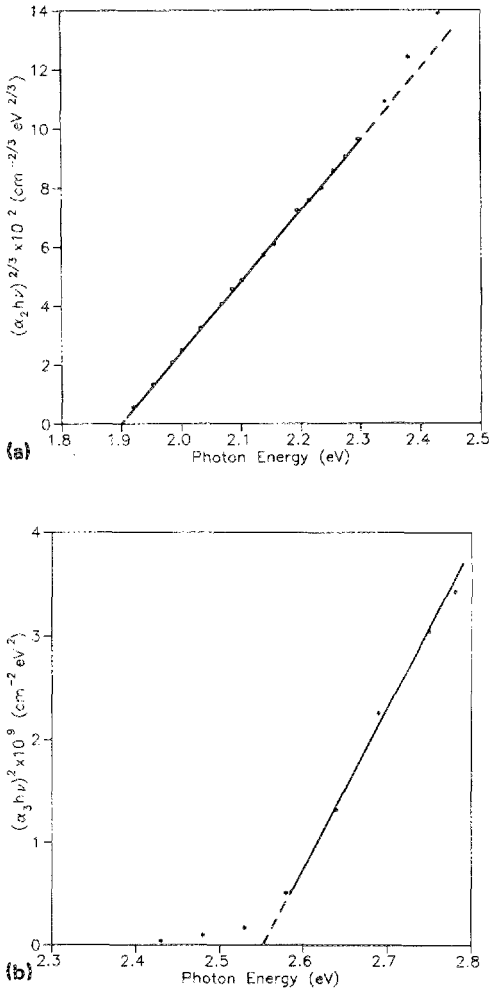

FIG. 9. (a) Additional analysis of optical absorption spectrum of data in Fig. 7 for direct forbidden transitions, Eq. (4) with $E_f = 1.90$ eV. (b) Additional analysis of optical absorption spectrum of data in Fig. 7 for direct allowed transitions, Eq. (5), with $E_a = 2.55$ eV.

in the literature for evaporated films.[7] None of the our sputtered CGS films showed the presence of the forbidden transition at 1.75 eV. This can be due to the fact that our CGS films were always Cu deficient, in agreement with the results reported by the S.E.R.I. group[23] which did not observe this transition in their Cu-poor material either. In fact, Cu-poor films seem to grow with the cubic, disordered structure. In this structure, the crystalline field interaction, responsible for the presence of the 1.75-eV transition, does not take place.[24]

It is clear from Fig. 9(a) that the presence of another transition takes place for energies higher than 2.30 eV. An analysis of the absorption in this energy range in terms of the relation

$$\alpha_3 = \alpha_{\text{exp}} - (\alpha_1 + \alpha_2) = (A_3/h\nu)\ (h\nu - E_a)^{1/2} \quad (5)$$

yielded an allowed direct transition at the energy value of $E_a = 2.55$ eV. Results are presented in Fig. 9(b). This transition was measured only in the thinnest ($t < 0.8\ \mu$m) films because of the very low transmittance values of the CGS at the higher photon energies.

The optical transitions quoted above showed a strong dependence on the growth temperature. E_g,E_f, and E_a values for all the films analyzed are presented in Fig. 10 as a function of growth temperature, showing at the lower growth temperature, values lower than those accepted for the single crystal.[22] In fact, at 60 °C, values as low as 1.62, 1.80, and 2.40 eV for the above-mentioned transitions are obtained. At the higher growth temperature, data were very close to the single-crystal values [see Figs. 8, 9(a) and 9(b)]. A similar behavior has been observed in sputtered $CuInSe_2$ thin films.[25] As in the electrical properties, the amorphous or poorly crystalline nature of CGS films grown at the lower growth temperatures causes the presence of a large quantity of gap states. As a consequence, optical transitions take place between those gap states thus reducing the optical gap E_g and the additional E_f and E_a transitions. In this way, structural characteristics are mainly responsible for the optical properties of our sputtered CGS films.

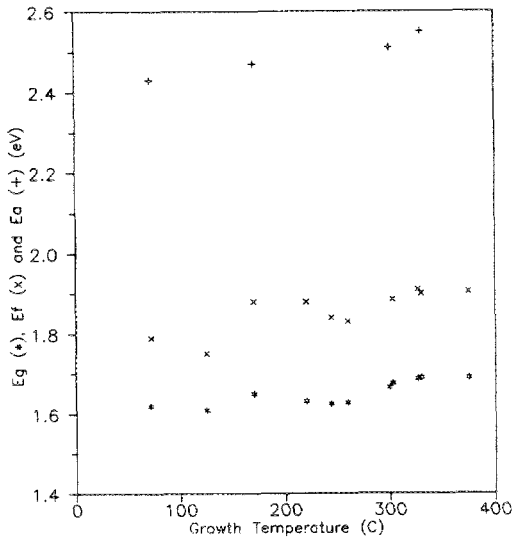

FIG. 10. Values of allowed fundamental transitions (E_g, *), forbidden direct transitions (E_f, ×), and allowed direct transitions (E_a +) as a function of the growth temperature.

IV. CONCLUSIONS

Structural, compositional, electrical, and optical properties of rf sputtered CGS thin films have been analyzed as a function of the growth temperature. Poorly crystalline, Se-rich films have been obtained at low growth temperatures, with the presence of binary phases. At the high growth temperatures ($T > 300$ °C), single-phase tetragonal CGS polycrystalline films, with average on grain size of about 0.7 μm in films that are Cu-poor and with Se/Cu + Ga ratios near to 1, were obtained. Electrical and optical properties were also strongly influenced by the growth temperature. All the films analyzed showed the presence of a hopping conduction mechanism at the lower measurement temperature, and a thermally activated processes over grain boundaries at the higher measurement temperature. The hopping conduction mechanism analysis revealed the presence of a great amount of structural defects in films grown at the lower growth temperature. On the other hand, films grown at higher growth temperature showed less structural defects. Structural defects together with film composition explain the strong decrease observed in the resistivity, when growth temperature was raised. Optical properties of CGS sputtered films showed the presence of the fundamental allowed direct transitions (E_g), forbidden direct transitions (E_f), and additional allowed direct transitions (E_a). E_g, E_f, and E_a values are strongly dependent on growth temperature. At the lower ones, optical transitions values are lower than those of single crystal, becoming closer to single-crystal values when the substrate temperature was raised. This behavior can be explained in terms of a reduced density of defect states in films grown at the higher growth temperatures.

ACKNOWLEDGMENTS

The authors would like to express their acknowledgment to J. Carabe (Instituto de Energias Renovables, C.I.E.-M.A.T.) for optical measurements facilities and J. M. Gomez de Salazar (Departamento de Metalurgia, U.C.M.) for S.E.M. observations and EDAX analysis. This work was partially supported by the U.S.–Spain Joint Committee for Science and Technology under Grant No. CCA-8411046.

[1] W. H. Bloss, J. Kimmerle, F. Pfisterer, and H. W. Schock, in *Proceedings of the 17th IEEE Photovoltaic Specialists Conference*, Kissimmee, FL, 1984 (IEEE, New York, 1984), p. 715.
[2] K. R. Murali, B. S. V. Gopalam, and J. Sobhandri, J. Mater. Sci. Lett. **5**, 421 (1986).
[3] R. Noufi, R. Powell, C. Herrington, and T. Coutts, Solar Cells **17**, 303 (1986).
[4] J. L. Annapurna and K. V. Reddy, Indian J. Pure Appl. Phys. **24**, 283 (1986).
[5] Y. K. Kapur, B. M. Basol, and E. S. Tseng, in *Proceedings of the 18th IEEE Photovoltaic Specialists Conference*, Las Vegas, NV, 1985 (IEEE, New York, 1986), p. 1429.
[6] W. Arnat, B. Dimmler, H. Dittrich, J. Kimerle, R. Menner, F. Pfisterer, and H. W. Schock, in *Proceedings of the 18th IEEE Photovoltaic Specialists Conference*, Las Vegas, NV, October 1985 (IEEE, New York, 1986).
[7] W. Horig, H. Neumann, B. Schumann, and G. Kuhn, Phys. Status Solidi B **85**, K57 (1978).

[8]I. Martil, G. Gonzalez-Diaz, J. Santamaria, M. L. Lucia, J. L. Hernandez-Rojas, and F. Sanchez-Quesada, J. Mater. Sci. Lett. (in press).
[9]I. Martil, G. Gonzalez-Diaz, and F. Sanchez-Quesada, Thin Solid Films **114**, 327 (1984).
[10]I. Martil, G. Gonzalez-Diaz, and F. Sanchez-Quesada, Solar Energy Mater. **12**, 345 (1985).
[11]ASTM Cards Numbers: 31-456 and 29-628.
[12]W. Arndt, H. Dittrich, and H. W. Schock, Thin Solid Films **130**, 209 (1985).
[13]J. Y. W. Seto, J. Appl. Phys. **46**, 5247 (1975).
[14]J. W. Orton and H. J. Powell, Rep. Prog. Phys. **43**, 1263 (1980).
[15]G. Masse, J. Phys. Chem. Solids **45**, 1091 (1984).
[16]L. Mandel, Solid State Commun. **32**, 201 (1979).
[17]M. H. Brodsky, ed., *Amorphous Semiconductors*, Vol. 36 of *Topics in Applied Physics* (Springer, Berlin, 1979).
[18]J. J. Hauser, Phys. Rev. Lett. **29**, 476 (1979).
[19]R. P. Sharma, A. K. Shukla, A. K. Kapoor, R. Srivastava, and P. C. Mathur, J. Appl. Phys. **57**, 2026 (1985).
[20]G. D. Boyd, H. M. Kasper, J. H. McFee, and F. G. Storz, IEEE J. Quantum Electron. **QE-8**, 900 (1972).
[21]I. Martil, G. Gonzalez-Diaz, F. Sanchez-Quesada, and M. Rodriguez-Vidal, Thin Solid Films **120**, 31 (1984).
[22]J. L. Shay, B. Tell, H. M. Kasper, and L. M. Schiavone, Phys. Rev. B **5**, 5003 (1972).
[23]J. Tuttle, D. Albin, J. Goral, C. Kennedy, and R. Noufi, Solar Cells **24**, 67 (1988).
[24]D. Albin, R. Noufi, J. Tuttle, J. Goral, and S. H. Risbud, J. Appl. Phys. **64**, 4103 (1988).
[25]J. Santamaria, I. Martil, Iborra, G. Gonzalez-Diaz, and F. Sanchez-Quesada, J. Vac. Sci. Technol. A **7**, 1424 (1989).